Large area laser-induced periodic surface structures on steel by bursts of femtosecond pulses with picosecond delays

Giuseppe Giannuzzi[a,b,*], Caterina Gaudiuso[a,b], Cinzia Di Franco[b], Gaetano Scamarcio[a,b], Pietro Mario Lugarà[a,b], Antonio Ancona[b]

[a]Università degli Studi di Bari, Dipartimento Interuniversitario di Fisica, via Amendola 173, I-70126 Bari, Italy

[b]Istituto di Fotonica e Nanotecnologie (IFN)-CNR U.O.S. Bari, via Amendola 173, I-70126 Bari, Italy

*Corresponding author: giuseppe.giannuzzi@uniba.it

Abstract

Bursts of linearly polarized femtosecond laser pulses with variable intra-burst delays on the picosecond timescale and different number of sub-pulses were used to produce laser-induced periodic surface structures (LIPSS) on stainless steel surfaces. The influence of the number and time spacing of sub-pulses on the LIPSS spatial period and depth has been systematically investigated. Scanning electron and atomic force microscopies revealed that, in case of bursts with only two sub-pulses, an increase of the intra-burst delay produces nanoripples with higher spatial separations but shallower depths which is ascribed to a shielding effect. Increasing the number of sub-pulses, a slight increase of the LIPSS spatial period has been observed.

Keywords: Laser structuring, nanostructures, laser-induced periodic surface structures, femtosecond laser, burst, metals

1. Introduction

When linearly polarized ultrashort laser pulses irradiate metallic surfaces, shallow periodic corrugations, known as laser-induced periodic surface structures (LIPSS), are generated. These ripples have sub-micrometric spatial periods, which makes them very attractive for many applications where it is required to change or control wettability [1], color [2], friction [3], absorptivity [4], and cells/bacteria adhesion [5] properties of technical surfaces.

It is still debated if LIPSS are generated in the early stage of the laser-matter interaction or, rather, after energy deposition and consequent self-reorganization of the material. Depending on their spatial frequency, LIPSS are classified into low spatial frequency LIPSS (LSFL), having a periodicity slightly lower than the laser wavelength, and high spatial frequency LIPSS (HSFL) with much smaller spatial separations [6]. The latter are mostly generated by irradiation with laser pulses of durations in the fs-ps range. Their origin is still unclear and the experimental control of their morphology remains a challenge. For the LSFL it

is generally recognized that, in case of metals, they are originated by the interaction of the incident laser light with the surface-scattered electromagnetic waves involving the excitation of surface plasmon polaritons [6,7]. The LSFL orientation is usually perpendicular to the laser polarization either in metals or semiconductors. Controlling size, orientation, period and depth of these shallow nanostructures has recently become a strategic goal for industrial applications.

Several experimental studies on the effect of laser irradiation conditions on the LIPSS morphology have been reported. In several cases, such works have confirmed the theoretical models which describe the physical mechanisms behind the formation of the LIPSS [8,9]. In particular, it was found that the LSFL spatial period is proportional to the incident laser wavelength λ [10]. Therefore, it was demonstrated that the ripples frequency can be varied either in a discrete way by using the higher harmonics of the laser or continuously by tuning the laser wavelength through an optical parametric amplifier (OPA). With this method Li et al. were able to tune the spatial period of the LIPSS produced on titanium and stainless steel samples in the range from 400 nm to 1600 nm [2,11]. However, employing such a sophisticated system as an OPA to control the LIPSS morphology is not viable in real production. The ripples periodicity changes also with the angle of incidence of the laser beam to the surface. This relationship was theoretically predicted by Bonch-Bruevich et al. [10] both in case of p- and s- polarized light and experimentally observed in several studies [6,11,12]. In [12] the ripples spatial period was tuned from ~500 nm to 4000 nm by changing the incidence angle from 0° to 70° in case of irradiation of stainless steel with p-polarized light. However, getting away from normal incidence conditions makes the morphology of the ripples more and more asymmetric until they resemble that of a blazed grating [13].

LIPSS formation occurs only in a certain laser fluence range just above the material damage threshold and below higher ablative regimes where the ripples are completely canceled [14]. The dose of laser energy deposited per unit area in terms of fluence and number of pulses per spot not only influences the LIPSS formation but also their morphology. In [14], an increase of the LIPSS period with the laser fluence was observed on metallic targets, in agreement with the theoretical model proposed in [15].

The number of pulses impinging on the same spot has been found to influence the type of LIPSS generated, i.e. HSFL or LSFL [16,17] and their spatial frequency. Bonse et al. [17] showed that the period of LSFL produced on titanium targets decreased from 750 nm to 520 nm by increasing the number of pulses from 1 to 1000 and keeping the same fluence. Nevertheless, most of the studies performed so far on the influence of the number of pulses and laser fluence on the LIPSS morphology have investigated what happens inside an ablation crater upon changing of the irradiation conditions. Few experimental data are available on the control of the LIPSS period by changing the laser fluence or the repetition rate when scanning the beam over large areas. Besides the irradiation conditions, also the ambient pressure may affect the LIPSS morphology. In [18], it was observed that the LIPSS periodicity on silicon can be increased by changing the

environmental pressure from atmospheric to high vacuum conditions. However, producing LIPSS with desired features in controlled atmosphere is impractical at an industrial level.

A promising approach to control the LIPSS morphology relies on tailoring the laser energy transfer to the material in the time domain. In recent studies on irradiation with double fs-pulses with different delays and/or wavelengths it was found that varying delay, polarization and energy ratio of the two sub-pulses allows to change the LIPSS orientation [18–20], with negligible impact on their period and depth [21,22]. Specifically, Fraggelakis et al. [20] showed the combined effect of the intrapulse ps-delay and the order of arrival of the cross-polarized double pulse sequence on the final LIPSS morphology. In addition, they found that the ripples orientation is mostly influenced by the polarization of the second pulse. The LIPSS periodicity on silicon [21] and fused silica [22] was found to decrease with the time separation between the two sub-pulses in the range from 0 to 40 ps. In the latter case also the ripples depth decreased with the delay [22]. In the aforementioned works, quite complex set-ups were used to split the pristine pulses, very sensitive to misalignments and thus hardly exploitable in industrial laser systems.

The influence of further splitting the laser pulses into higher numbers of sub-pulses, so-called burst mode processing, on the LIPSS formation has not been explored, yet.

In this work, we report on the morphology of LSFL produced by irradiating stainless steel targets with bursts of variable numbers of femtosecond laser sub-pulses, having the same linear polarization and intra-burst delays in the ps range. The set-up used for the generation of the bursts, based on a cascade of birefringent crystals, was almost insensitive to beam misalignment and thus very robust for industrial use, and offered great flexibility in terms of pulse splitting and selectable intrapulse delay. First, we focused on bursts of two sub-pulses with different delays. Then, the pristine laser pulses were split into a number of up to 32 sub-pulses per burst, and the influence of the intra-burst delay and the number of sub-pulses per burst onto the ripples spatial frequency and depth was systematically investigated.

2. Experimental details

The outline of the setup used to generate bursts of femtosecond pulses with picosecond delays and produce large area laser-induced periodic surface structures on steel samples is shown in Fig. 1.

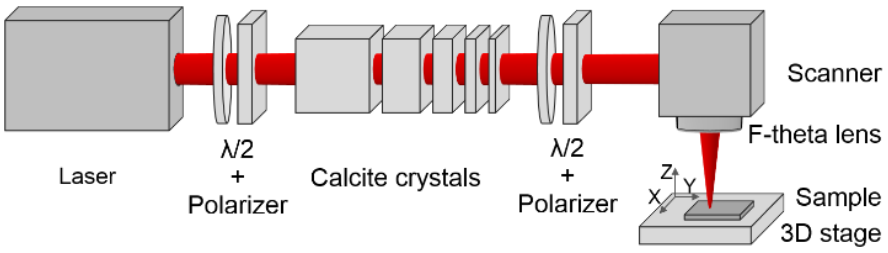

Fig. 1. Schematic of experimental setup. The number of sub-pulses and the time delay within the burst depends on the crystals order and orientation with respect to the polarization direction of the incident pulses [23].

A compact Yb:KGW femtosecond laser system (PHAROS from Light Conversion), built upon conventional chirped pulse amplification technique, was used to deliver pulses with duration of 238 fs, central wavelength λ = 1030 nm, maximum pulse energy 1.5 mJ, and variable repetition rate from single pulse to 1 MHz. The repetition rate was set to 200 kHz. Bursts have been produced by splitting the pristine linearly polarized laser pulses by means of an array of five birefringent calcite crystals. The number *n* of sub-pulses with equally fractioned energy, from 2 to 32, their polarization and the intra-burst delay depend on the order in which the crystals are arranged and how the optical axis of each crystal is oriented with respect to the polarization direction of the incident pulse [23].The total energy per burst and, accordingly, the sub-pulses energy was finely adjusted by means of a half-wave plate and a polarizer placed upstream of the calcite crystals. The sub-pulses emerge from the crystals with orthogonal polarizations. A further half-wave plate followed by a polarizer were positioned after the crystals array to obtain bursts of sub-pulses with known and parallel linear polarization. This was due in order to avoid that, in case of cross-polarized sub-pulses, the imprint of the last sub-pulse polarization state could affect the final ripples orientation [18,20]. Table 1 summarizes the selected burst features for each experiment performed in this study.

Table 1.

Burst features of the conducted experiments.

Experiment	Number of sub-pulses in the burst	Time separation between sub-pulses
1)	n = 2	Δt = 1.5-3-6-12-24 ps
2)	n = 2-4-8-16-32	Δt = 1.5 ps

Polished stainless steel (AISI 301) samples were irradiated over an area of 6 mm^2 using a Galvo Scanner system (SCANLAB's intelliSCAN 14) equipped with a 56 mm focal length F-theta lens. The focused spot size measured on the sample surface was 24 μm ($1/e^2$ peak intensity). The irradiated area was centered with the F-Theta lens scan field to ensure normal incidence of the beam to the sample surface. The scanning direction was always kept perpendicular to the beam polarization; the scanning speed and the offset between line scans were adjusted to 1 m/s and 10 μm, respectively, to produce uniform patterns over the whole irradiated area. All experiments have been performed in ambient air.

A fixed burst fluence of 0.85 J/cm^2 was employed during all the experiments, since this value was found to enable LIPSS formation with any burst feature investigated. For comparison, analogous surface structuring experiments have been performed with unsplit pristine laser pulses, indicated in the following as Normal Pulse Mode (NPM), with same laser fluence and scanning scheme.

After processing, all the surfaces were characterized by scanning electron microscopy (FE-SEM, Carl Zeiss mod. Σigma, Germany) and atomic force microscopy (AFM, NT-MDT mod. Ntegra, Russia). The SEM images

were acquired at an accelerating voltage of 1 kV and a working distance of 2.5 mm using the InLens detector, and subsequently analyzed by a 2D-Fourier transform algorithm to evaluate the ripples spatial frequency. The 2D Fourier spectrum results were averaged over five repeated acquisitions on different areas of the same surface. The LIPSS depth Δz was derived from the AFM images acquired in semi-contact mode using a tip apex size of 10 nm at a frequency f = 263 kHz. For each sample produced with different burst features, a representative area of 30 µm x 4 µm was investigated.

3. Results and discussion

Figure 2 shows representative SEM images of the LIPSS generated by the burst irradiation conditions selected in our study, i.e. double femtosecond pulses (n=2) with parallel linear polarization (oriented along the double arrow in the image) and variable delays from 24 ps to 1.5 ps (Fig. 2a-e) and bursts with increasing number of sub-pulses from n=2 to 32 and fixed intraburst delay of 1.5 ps (Fig. 2e-i). All the samples produced with different bursts features exhibited the same type of ripples: LSFL oriented perpendicular to the laser beam polarization, evenly distributed over large areas and having a spatial period close to the laser wavelength. Especially the LSFL produced using bursts with shorter delays appeared well defined, highly regular and homogeneous all over the irradiated area (see Fig. 2e), while for longer time separations between sub-pulses shallower and more unevenly distributed structures were observed (see Fig. 2a).

Within the LSFL also HSFL were noticed, but only in a few cases when bursts with relatively high number of sub-pulses were used. When present, HSFL were located along the LSFL valleys and aligned parallel to the laser polarization (see insets in Fig. 2h-i). Our study was thus aimed at investigating if the morphology of the LSFL changed with the variation of the bursts parameters n and Δt.

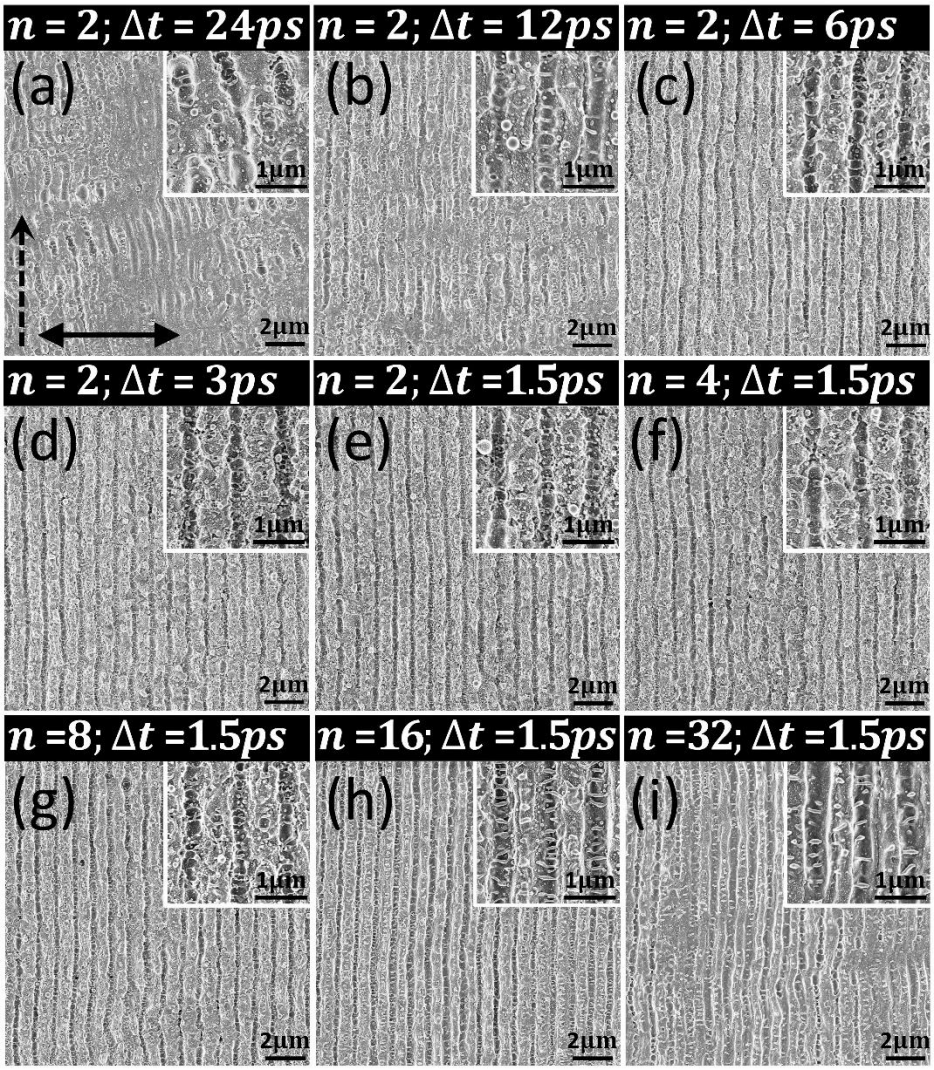

Fig. 2. SEM micrographs of the stainless steel surface irradiated by bursts. The images (a-e) are relative to bursts of double sub-pulses and decreasing time separation: (a) Δt = 24 ps, (b) Δt = 12 ps, (c) Δt = 6 ps, (d) Δt = 3 ps and (e) Δt = 1.5 ps. From (e) to (i) the time separation is fixed at 1.5 ps while increases the number of sub-pulses inside the burst: (e) n = 2, (f) n = 4, (g) n = 8, (h) n = 16 and (i) n = 32. The inset pictures show a zoomed view of the ripples. HSFLs are clearly observed for the texturized surface by burst with n > 4. The double arrow indicates the direction of pulses polarization while the dotted arrow the laser scanning direction.

Starting from the SEM images acquired on diverse areas on the same samples produced with different burst parameters, the LSFL spatial periods were derived by a 2D-Fourier transform algorithm. As an example, in figure 3a a SEM image of the LSFL generated using bursts of n = 16 sub-pulses with intra-burst delay of Δt = 1.5 ps is reported while in figure 3b the related 2D-Fourier Transform spectrogram is shown.

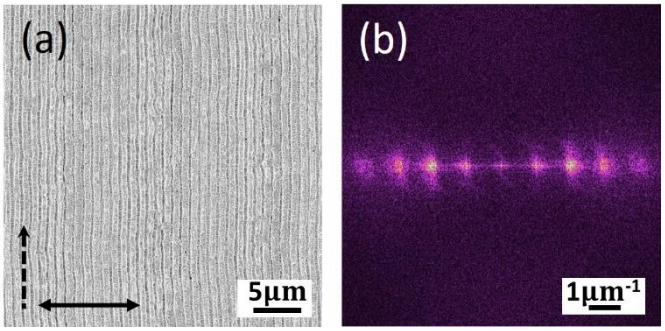

Fig. 3. (a) SEM micrograph of the stainless steel surface irradiated by burst of n = 16 sub-pulses delayed of Δt = 1.5 ps. The double arrow indicates the polarization axis of the impinging sub-pulses, while the dotted arrow shows the beam scanning direction. (b) 2D-Fourier Transform of the SEM image.

Here, the bright dots represent the maximum spatial frequency values and their distance from the center of the image is used to evaluate the ripples spatial frequency.

For the LSFL depths Δz, an appositively developed algorithm analyzed the AFM profiles (see for example Fig. 4a) and estimated the peak-to-valley height of the ripples over the whole examined area. First, the algorithm located the highest and lowest points along each line of pixels perpendicular to the ripples orientation (Fig. 4b). Then, the peaks-to-valley depths were calculated and plotted on a histogram. From the Gaussian fit of all the data, it was possible to precisely estimate the averaged ripples depth Δz and the corresponding standard deviation (Fig. 4c).

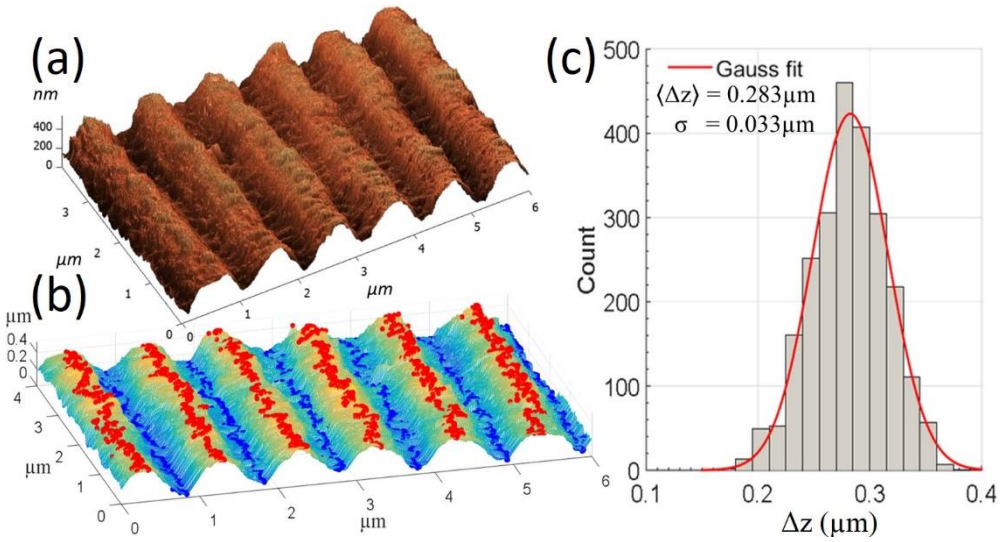

Fig. 4. (a) AFM image of a surface irradiated by burst of 16 sub-pulses delayed of 1.5 ps. By algorithm, the peak and valley points of the ripples was located (b). The depths of adjacent peak-valley were calculated and plotted in a histograms (c) which was fitted by a Gaussian fit.

All the data gathered on the LSFL morphology produced under different burst irradiation conditions are further discussed in the following.

Figure 5 reports the spatial period (Λ) and depth (Δz) of the ripples generated by bursts of just 2 sub-pulses with variable delays Δt, ranging from 1.5 ps to 24 ps (experiment 1 of table 1). In the same graph, results of period and depth for LIPSS generated by NPM (Δt = 0 ps) are also shown, which are similar to the values reported by analogous experiments conducted on stainless steel targets [7].

For intra-burst delays shorter than 6 ps the ripples spatial period is close to the value of 900 nm found in NPM, while it increases for longer delays up to 944 nm for Δt = 24 ps. The depth of the ripples is always smaller than the NPM case, although for Δt shorter than 6 ps it stays almost constant around 240 nm, very close to the value measured with unsplit pulses. For longer time separations between the two sub-pulses the depth progressively decreases, being more than halved for Δt = 24 ps.

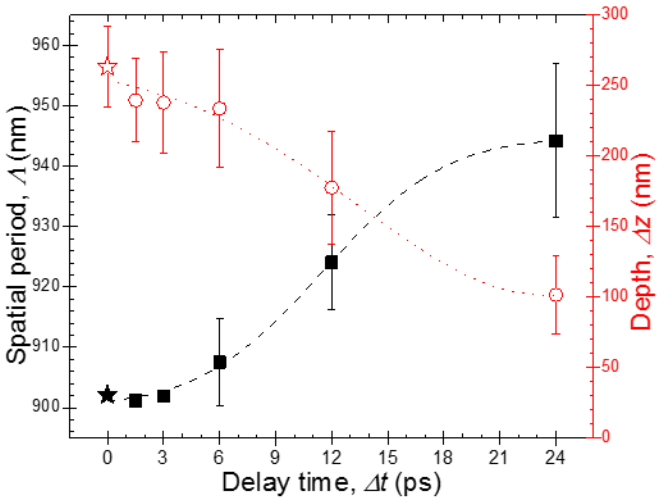

Fig. 5. Variation of the LSFL period (Λ, ■) and depth (Δz, ○) as a function of the time delay Δt between two sub-pulses. The points (⋆, ✯) at Δt = 0 ps represent the normal pulse mode case.

The decrease of the ripples depth with the time separation between the two sub-pulses can be ascribed to a plasma shielding effect, as also reported in case of an ablation crater produced by double laser pulses [24]. Indeed, the interaction of the first sub-pulse with the surface generates a plasma that absorbs or diffuses part of the radiation from the incoming second sub-pulse, thus reducing the overall energy impinging on the sample. Our results suggest that for delays shorter than 6 ps between sub-pulses, such effect is negligible since the plasma is still at an early stage of formation. As the time separation between sub-pulses increases, the plasma shielding effect becomes more prominent thus producing shallower ripples compared to the case of unsplit pulses.

Following this interpretation, even shallower structures were expected by increasing the pulse splitting and the number of sub-pulses in the bursts. Figure 6 shows results of the LSFL periodicity and depth obtained with bursts of growing numbers of sub-pulses n from 2 to 32, and fixed intra-burst delay Δt = 1.5ps. Here,

the ripples depth decreases from 240 nm for n = 2 to 210 nm for n = 4, but then start increasing again above 260 nm for n = 8 and n = 16, thus indicating that a second physical mechanism occurs which compensates for the plasma shielding effect. This mechanism is probably incubation, which has been already demonstrated to be responsible for a lowering of the surface damage threshold fluence in case of irradiation with bursts of increasing number of sub-pulses [25]. Further splitting up to n = 32 results into shallower LSFL, apparently because of the much less energy available for each sub-pulse to produce material surface modifications.

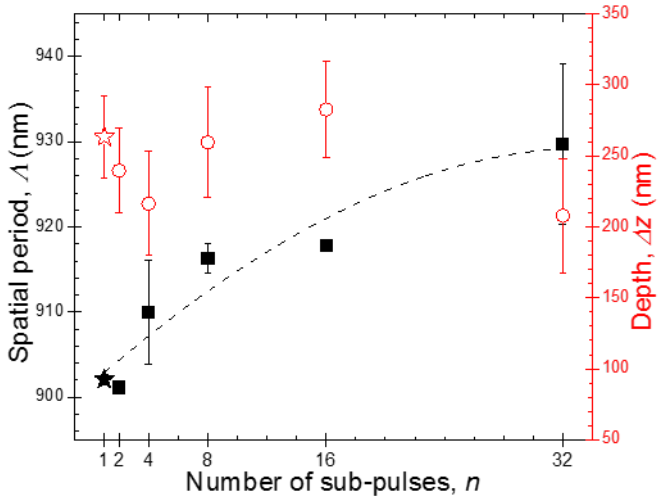

Fig. 6. Variation of the LSFL period (Λ, ■) and depth (Δz, ○) as a function of the number of sub-pulses n in the burst at fixed time delay (Δt = 1.5ps). The points (⋆, ⋆) at n = 1 represent the normal pulse mode case.

Figure 6 also shows a steady increase of the LSFL spatial period with the number of sub-pulses in the burst. It is thus confirmed that bursts always produce ripples with spatial periods larger than NPM. In a previous study it has been proposed that in case of irradiation with multiple pulses the grating-like structure generated by the first few laser pulses may influence the coupling of the laser radiation with the surface plasmon polariton, leading to a shift in the LSFL period [26]. However, understanding the physical mechanism behind this effect still deserves further experimental investigations.

4. Conclusions

The generation of LIPSS on steel samples irradiated by bursts of linearly polarized ultrashort laser pulses with same fluence and variable number of sub-pulses and intra-burst delays has been systematically investigated. The time separations between sub-pulses in the bursts were in the range of several picoseconds, corresponding to the timescale of the electron-phonon coupling time in metals. It was found that the LSFL frequency and depth changes with the burst features. For bursts consisting of two sub-pulses, the spatial period increases with the intra-burst delay, while the ripples depth decreases due to a plasma shielding effect. The latter mechanism is compensated by incubation when the number of sub-pulses in the

burst is higher thus leading to ripples with nearly same depth, whereas the spatial period increases with the pulse splitting. Understanding the physical mechanism behind the change of the LSFL periodicity with the burst features *n* and *Δt* deserves further investigations. Nonetheless, our study suggests that regular patterns of nano-ripples evenly distributed over large metallic surface areas can be produced using burst of ultrashort laser pulses and that the spatial period and depth of such surface nanostructures can be finely controlled by adjusting the burst characteristics. In principle, this approach is much more robust and convenient than other techniques used for the same purpose, which are not suitable for industrial applications since they are based on the use of expensive equipment like OPA or complicated setups requiring precise control of the ambient pressure or the angle of incidence of the laser beam onto the surface. While the solution proposed in this work is based on a cheap and flexible setup consisting of an array of birefringent crystals that can be easily adapted to any ultrafast laser source, thus opening up new possibilities in many application fields where it is crucial to precisely tailor the optical, wettability, adhesion and frictional properties of metal surfaces.

Acknowledgment

This research was partially supported by the APULIA Region for funding the regional laboratories network MICROTRONIC (cod. 71). G.S. acknowledges support from PON SISTEMA (MIUR). The authors wish to thank Tecno Acciai S.r.l. for the provision of the high quality steel samples.

References

[1] Müller FA, Kunz C, Gräf S. Bio-inspired functional surfaces based on laser-induced periodic surface structures. Materials (Basel) 2016;9. doi:10.3390/ma9060476.

[2] Li G, Li J, Hu Y, Zhang C, Li X, Chu J, et al. Femtosecond laser color marking stainless steel surface with different wavelengths. Appl Phys A Mater Sci Process 2014;118:1189–96. doi:10.1007/s00339-014-8868-3.

[3] Wang Z, Zhao Q, Wang C. Reduction of friction of metals using laser-induced periodic surface nanostructures. Micromachines 2015;6:1606–16. doi:10.3390/mi6111444.

[4] Ou Z, Huang M, Zhao F. The fluence threshold of femtosecond laser blackening of metals: The effect of laser-induced ripples. Opt Laser Technol 2016;79:79–87. doi:10.1016/j.optlastec.2015.11.018.

[5] Martínez-Calderon M, Manso-Silván M, Rodríguez A, Gómez-Aranzadi M, García-Ruiz JP, Olaizola SM, et al. Surface micro- and nano-texturing of stainless steel by femtosecond laser for the control of cell migration. Sci Rep 2016;6:1–10. doi:10.1038/srep36296.

[6] Bonse J, Höhm S, Kirner S V., Rosenfeld A, Krüger J. Laser-induced periodic surface structures – a scientific evergreen. IEEE J Sel Top Quantum Electron 2017;23:9000615. doi:10.1109/jstqe.2016.2614183.

[7] Gnilitskyi I, Derrien TJY, Levy Y, Bulgakova NM, Mocek T, Orazi L. High-speed manufacturing of highly regular femtosecond laser-induced periodic surface structures: Physical origin of regularity. Sci Rep 2017;7:1–11. doi:10.1038/s41598-017-08788-z.

[8] Sipe JE, Young JF, Preston JS, Van Driel HM. Laser-induced periodic surface structure. I. Theory. Phys Rev B 1983;27:1141–54. doi:10.1103/PhysRevB.27.1141.

[9] Bonse J, Rosenfeld A, Krüger J. On the role of surface plasmon polaritons in the formation of laser-induced periodic surface structures upon irradiation of silicon by femtosecond-laser pulses. J Appl Phys 2009;106. doi:10.1063/1.3261734.

[10] Bonch-Bruevich AM, Libenson MN, Makin VS. Surface electromagnetic waves in optics. Opt Eng 1992;31:718–25.

[11] Li G, Li J, Li X, Zhu Z, Hu Y, Chu J, et al. Evolution of Titanium Surfaces Irradiated by Femtosecond Laser Pulses with Different Wavelengths. Proc. SPIE, vol. 8769, 2013, p. 87691V–1–5. doi:10.1117/12.2021098.

[12] Nürnberger P, Reinhardt H, Kim HC, Yang F, Peppler K, Janek J, et al. Influence of substrate microcrystallinity on the orientation of laser-induced periodic surface structures. J Appl Phys 2015;118. doi:10.1063/1.4932215.

[13] Hwang TY, Guo C. Femtosecond laser-induced blazed periodic grooves on metals. Opt Lett 2011;36:2575. doi:10.1364/OL.36.002575.

[14] Okamuro K, Hashida M, Miyasaka Y, Ikuta Y, Tokita S, Sakabe S. Laser fluence dependence of periodic grating structures formed on metal surfaces under femtosecond laser pulse irradiation. Phys Rev B - Condens Matter Mater Phys 2010;82:1–5. doi:10.1103/PhysRevB.82.165417.

[15] Sakabe S, Hashida M, Tokita S, Namba S, Okamuro K. Mechanism for self-formation of periodic grating structures on a metal surface by a femtosecond laser pulse. Phys Rev B - Condens Matter Mater Phys 2009;79:1–4. doi:10.1103/PhysRevB.79.033409.

[16] Hsu EM, Crawford THR, Tiedje HF, Haugen HK. Periodic surface structures on gallium phosphide after irradiation with 150 fs-7 ns laser pulses at 800 nm. Appl Phys Lett 2007;91:2005–8. doi:10.1063/1.2779914.

[17] Bonse J, Höhm S, Rosenfeld A, Krüger J. Sub-100-nm laser-induced periodic surface structures upon irradiation of titanium by Ti:sapphire femtosecond laser pulses in air. Appl Phys A Mater Sci Process 2013;110:547–51. doi:10.1007/s00339-012-7140-y.

[18] Hashida M, Nishii T, Miyasaka Y, Sakagami H, Shimizu M, Inoue S, et al. Orientation of periodic grating structures controlled by double-pulse irradiation. Appl Phys A Mater Sci Process 2016;122:1–5. doi:10.1007/s00339-016-0011-1.

[19] Furukawa Y, Sakata R, Konishi K, Ono K, Matsuoka S, Watanabe K, et al. Demonstration of periodic nanostructure formation with less ablation by double-pulse laser irradiation on titanium. Appl Phys

Lett 2016;108:1–5. doi:10.1063/1.4955035.

[20] Fraggelakis F, Stratakis E, Loukakos PA. Control of periodic surface structures on silicon by combined temporal and polarization shaping of femtosecond laser pulses. Appl Surf Sci 2018;444:154–60. doi:10.1016/j.apsusc.2018.02.258.

[21] Tsibidis GD, Stratakis E, Loukakos PA, Fotakis C. Controlled ultrashort-pulse laser-induced ripple formation on semiconductors. Appl Phys A Mater Sci Process 2014;114:57–68. doi:10.1007/s00339-013-8113-5.

[22] Rosenfeld A, Rohloff M, Höhm S, Krüger J, Bonse J. Formation of laser-induced periodic surface structures on fused silica upon multiple parallel polarized double-femtosecond-laser-pulse irradiation sequences. Appl Surf Sci 2012;258:9233–6. doi:10.1016/j.apsusc.2011.09.076.

[23] Dromey B, Zepf M, Landreman M, O'keeffe K, Robinson T, Hooker SM. Generation of a train of ultrashort pulses from a compact birefringent crystal array. Appl Opt 2007;46:5142–6. doi:10.1364/AO.46.005142.

[24] Semerok A, Dutouquet C. Ultrashort double pulse laser ablation of metals. Thin Solid Films 2004;453–454:501–5. doi:10.1016/j.tsf.2003.11.115.

[25] Gaudiuso C, Giannuzzi G, Volpe A, Lugarà PM, Choquet I, Ancona A. Incubation during laser ablation with bursts of femtosecond pulses with picosecond delays. Opt Express 2018;26:3801. doi:10.1364/OE.26.003801.

[26] Huang M, Zhao F, Cheng Y, Xu N, Xu Z. Origin of laser-induced near-subwavelength ripples: Interference between surface plasmons and incident laser. ACS Nano 2009;3:4062–70. doi:10.1021/nn900654v.